Born approximation of acoustic radiation force used for acoustofluidic separation

Chirag A. Gokani, Thomas S. Jerome, Michael R. Haberman, et al.

Citation: Proc. Mtgs. Acoust. **48**, 045002 (2022); doi: 10.1121/2.0001646
View online: https://doi.org/10.1121/2.0001646
View Table of Contents: https://asa.scitation.org/toc/pma/48/1
Published by the Acoustical Society of America

Volume 48 http://acousticalsociety.org/

22nd International Symposium on Nonlinear Acoustics

Oxford, UK
4-8 July 2022

Physical Acoustics: Session 4 - Radiation Force

Born approximation of acoustic radiation force used for acoustofluidic separation

Chirag A. Gokani, Thomas S. Jerome, Michael R. Haberman, and Mark F. Hamilton
Applied Research Laboratories, The University of Texas at Austin, Austin, Texas 78713-8029, USA; Walker Department of Mechanical Engineering, The University of Texas at Austin, Austin, Texas 78712-1063; chiragokani@utexas.edu; tsjerome@utexas.edu; haberman@utexas.edu; hamilton@mail.utexas.edu

Acoustofluidic separation often involves biological targets with specific acoustic impedance similar to that of the host fluid, and with dimensions up to the order of a wavelength. This parameter range, combined with the use of standing waves to separate the targets, lends itself to use of the Born approximation for calculating the acoustic radiation force. Considered here is the configuration analyzed by Peng et al. [J. Mech. Phys. Solids 145, 104134 (2020)], in which two intersecting plane waves radiated into the fluid by a standing surface acoustic wave exert a force on a eukaryotic cell modeled as a multilayered sphere. The acoustic field in this case has the structure of a standing wave parallel to the substrate and a traveling wave perpendicular to the substrate. For all parameter values considered by Peng et al., including spheres several wavelengths in diameter, the Born approximation of the acoustic radiation force parallel to the substrate is in good agreement with a full theory based on spherical wave expansions of the acoustic field. The importance of incorporating the internal structure of the cell is demonstrated by examining the counterexample of a homogenized sphere with uniform material properties obtained by volume averaging.

Published by the Acoustical Society of America

 https://doi.org/10.1121/2.0001646

1. INTRODUCTION

The use of acoustic radiation force for the separation of particles in microfluidic devices, i.e., acoustofluidic separation, has advanced significantly in recent years.[1] These types of systems are especially promising for application in the biological sciences. The acoustic radiation force is capable of manipulating cells without contact and with significantly reduced concern for negatively affecting their viability when compared to optical methods, and acoustofluidic devices are capable of rapidly sorting relatively large quantities of cells based on differences in their acoustic properties. In the design and modeling of acoustofluidic separation devices, accurate prediction of the acoustic radiation force exerted on cells in the separation process is desirable. Biological cells in particular are challenging to model using existing solutions for radiation force because they are typically inhomogeneous or nonspherical, and can have dimensions on the order of an acoustic wavelength.

In previous work, it was demonstrated that the Born approximation for acoustic radiation force is capable of accurately predicting the radiation force on inhomogeneous and nonspherical objects subject to an incident standing plane wave.[2–4] An analytical expression obtained using the Born approximation was compared with an existing solution for radiation force on a nucleated cell obtained by Wang et al.,[5] and the two approaches were observed to be in good agreement. The present work applies the Born approximation to the context of an acoustofluidic separation device. The Born approximation is applied to the device modeled by Peng et al.[6] and used to obtain an analytical expression for the radiation force on a sphere surrounded by an arbitrary number of concentric spherical layers. Results obtained from the Born approximation are compared with a full solution for radiation force for several of the cases considered in Ref. 6, and good agreement is observed for a wide range of object sizes and configurations of the incident field. It is shown that the component of the force predicted by the Born approximation is generally the dominant contribution to the acoustic radiation force for situations in which the Born approximation is expected to be accurate. To illustrate the importance of accounting for material inhomogeneity in the cell, comparisons are made between results for the multilayered cell and a homogenized sphere with uniform material properties obtained by volume averaging.

2. MODELS OF ACOUSTIC RADIATION FORCE FOR PARTICLE SEPARATION

The configuration of the acoustofluidic device modeled in the present work is that considered by Peng et al.[6] The device consists of a piezoelectric substrate over which lies a fluid half-space. If the sound speed c_0 in the fluid is less than the velocity c_R of a surface wave (leaky Rayleigh wave) propagating in the substrate, the surface wave will radiate a wave into the fluid at the Rayleigh angle θ_R determined by the ratio of the wave speeds:

$$\sin\theta_R = c_0/c_R, \tag{1}$$

where the angle θ_R is measured relative to the surface normal. In a standing surface acoustic wave device, two counterpropagating waves are radiated into the fluid and intersect at angle $2\theta_R$.

The incident acoustic pressure field $p = \frac{1}{2}p_{\text{in}}e^{-i\omega t} + \text{c.c.}$ generated by the standing surface acoustic wave device is represented by the superposition of two progressive plane waves $p_{\text{in}} = p_+ + p_-$ of the form $p_\pm = \frac{1}{2}p_0 e^{i\mathbf{k}_\pm\cdot\mathbf{r}}$. Defining a Cartesian coordinate system with the x axis normal to the substrate and the surface waves propagating along the z axis (see Fig. 1) yields the corresponding wave vectors $\mathbf{k}_\pm = k_0(\cos\theta_R\,\mathbf{e}_x \pm \sin\theta_R\,\mathbf{e}_z)$ where $k_0 = \omega/c_0$ is the wavenumber in the fluid. The complex pressure field in the fluid is thus given by

$$p_{\text{in}} = \tfrac{1}{2}p_0(e^{i\mathbf{k}_+\cdot\mathbf{r}} + e^{i\mathbf{k}_-\cdot\mathbf{r}}) \tag{2a}$$

$$= p_0\cos(k_0 z\sin\theta_R)e^{ik_0 x\cos\theta_R}. \tag{2b}$$

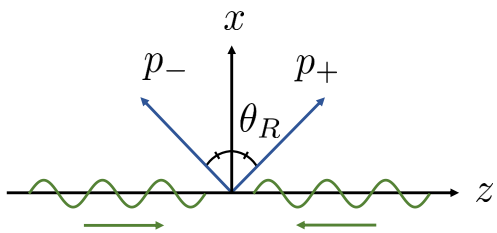

Figure 1: Sketch of the coordinate system and the propagation directions of the two plane waves p_+ and p_-. The standing surface acoustic wave is composed of two counterpropagating surface waves that travel along the z axis. The counterpropagating surface waves radiate corresponding plane waves into the fluid at the Rayleigh angle θ_R measured relative to the vertical x axis that is normal to the surface of the substrate in the y-z plane.

It can be seen by inspection of Eq. (2b) that the pressure field generated by the surface acoustic wave device has the structure of a standing wave parallel to the surface of the substrate along the z axis, but it forms a traveling wave in the x direction perpendicular to the substrate. Equation (2b) reduces to a pure progressive wave for $\theta_R = 0$, and to a pure standing wave for $\theta_R = 90°$. For a separation device with this configuration, the flow direction is along the y axis, which points out of the page in Fig. 1, and it is the standing wave structure that is responsible for the horizontal radiation force that causes the desired translation of particles perpendicular to the flow in the acoustofluidic separation process. As in Ref. 6, it is assumed that any surfaces above the substrate containing the fluid in the channel are acoustically transparent.

A. BORN APPROXIMATION OF ACOUSTIC RADIATION FORCE

The present work assesses the accuracy of the Born approximation of acoustic radiation force applied to the acoustic field described by Eq. (2). The form of the Born approximation employed here is that presented in Ref. 3, which expresses the radiation force on a scattering object as an integral over the volume of the object:

$$\mathbf{F} = -\int_V \left[f_K(\mathbf{r}) \boldsymbol{\nabla} \langle E_p \rangle - \tfrac{3}{2} f_\rho(\mathbf{r}) \boldsymbol{\nabla} \langle E_k \rangle \right] dV. \tag{3}$$

The quantities $\langle E_p \rangle$ and $\langle E_k \rangle$ are the time-averaged potential and kinetic energy densities of the incident field, and the contrast factors f_K and f_ρ are given by

$$f_K(\mathbf{r}) = \frac{K(\mathbf{r}) - K_0}{K(\mathbf{r})}, \qquad f_\rho(\mathbf{r}) = 2\frac{\rho(\mathbf{r}) - \rho_0}{2\rho(\mathbf{r}) + \rho_0}, \tag{4}$$

with ρ_0 and $K_0 = \rho_0 c_0^2$ the density and bulk modulus of the background fluid, respectively, and $\rho(\mathbf{r})$ and $K(\mathbf{r})$ the spatially dependent density and bulk modulus of the scatterer. The Born approximation in Eq. (3) applies to objects of arbitrary shape and inhomogeneity, subject to the restrictions outlined in Refs. 2 and 3. The primary restrictions are that the acoustic contrast between the object and the host fluid must be small, and that the incident field must not resemble too closely a progressive plane wave.

For the incident field defined in Eq. (2b), the time-averaged energy densities take the forms

$$\langle E_p \rangle = \frac{p_0^2}{4\rho_0 c_0^2} \cos^2(k_0 z \sin\theta_R), \tag{5}$$

$$\langle E_k \rangle = \frac{p_0^2}{4\rho_0 c_0^2} \left[\cos^2(k_0 z \sin\theta_R) \cos^2\theta_R + \sin^2(k_0 z \sin\theta_R) \sin^2\theta_R \right]. \tag{6}$$

Evaluation of Eq. (3) for the energy densities in Eqs. (5) and (6) yields the Born approximation of the force exerted on an object in the incident field described by Eqs. (2):

$$\mathbf{F} = -\int_V \frac{p_0^2 \tilde{k}_0}{4\rho_0 c_0^2} \tilde{f}_G(\mathbf{r}) \sin[2\tilde{k}_0(z+d)]\, \mathbf{e}_z \, dV. \tag{7}$$

The substitution $z \to (z+d)$ has been made in Eq. (7) to account for translation of the field in Eq. (2) relative to the object, which is nominally centered at $z = 0$, to simplify integration. Equation (7) is identical to Eq. (16) in Ref. 3 for a pure standing wave except for the substitutions $k_0 \to \tilde{k}_0$ and $f_G \to \tilde{f}_G$, where $\tilde{f}_G$ and $\tilde{k}_0$ are given by

$$\tilde{f}_G(\mathbf{r}) = f_K(\mathbf{r}) - \frac{3}{2} f_\rho(\mathbf{r}) \cos 2\theta_R, \qquad \tilde{k}_0 = k_0 \sin\theta_R. \tag{8}$$

Consequently, results for the pressure field generated by the surface acoustic wave device considered in the present work may be obtained from the corresponding results derived for a pure standing wave in Refs. 3 and 2 via a simple substitution to account for dependence of the acoustic contrast factor $\tilde{f}_G$ and effective wavenumber $\tilde{k}_0$ on the angle θ_R. For the case $\theta_R = 90°$, Eq. (7) reduces to Eq. (16) of Ref. 3.

The Born approximation in Eq. (7) only predicts a force that acts parallel to the surface of the substrate because it is associated with the gradients of the energy densities arising from the standing wave structure of the incident field. The vertical component of the force that acts in the direction of the surface normal is not accounted for in the Born approximation because it is associated with the progressive wave component of the acoustic field.[2] In the context of acoustofluidic separation the vertical force is of secondary concern, as the process is driven primarily by the horizontal radiation force.

The specific case of interest in the present work is that of a biological cell, modeled as a sphere surrounded by concentric spherical layers,[5,6] illustrated in Fig. 2. The Born approximation for the force on a multilayered sphere due to the field in Eq. (2) follows directly from the result derived previously for a pure standing plane wave[3] via the substitution described above:

$$F_z = \frac{\pi p_0^2}{2\rho_0 c_0^2} \sin 2\tilde{k}_0 d \left\{ \tilde{f}_{G1} R_1^2 j_1(2\tilde{k}_0 R_1) + \sum_{n=1}^{N} \tilde{f}_{G,n+1} \left[R_{n+1}^2 j_1(2\tilde{k}_0 R_{n+1}) - R_n^2 j_1(2\tilde{k}_0 R_n) \right] \right\}, \tag{9}$$

where j_1 is the spherical Bessel function of order 1. Equation (9) describes the horizontal radiation force on a sphere with acoustic contrast factor $\tilde{f}_{G1}$ and radius R_1 surrounded by N concentric spherical layers with contrast factor $\tilde{f}_{G,n}$ and outer radius R_n as shown in Fig. 2 for $N = 2$ layers.

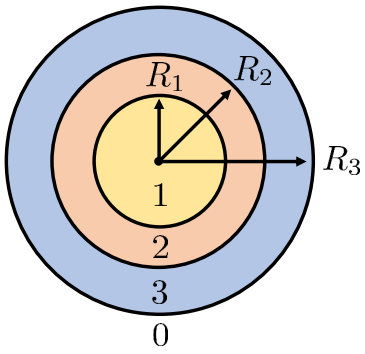

Figure 2: Sketch of the geometrical configuration of the nucleated cell considered in Refs. 5 and 6 and modeled in the present work using the Born approximation. The cell consists of an inner sphere with radius R_1 ***(region 1) surrounded by a layer of cytoplasm with outer radius*** R_2 ***(region 2) and an outer cortical layer with outer radius*** R_3 ***(region 3), and is suspended in a host fluid (region 0). The material properties are presented in Table 1.***

B. FULL SOLUTION FOR ACOUSTIC RADIATION FORCE

To assess the accuracy of the Born approximation when applied to acoustofluidic sorting of biological cells, results obtained using Eq. (9) are compared with the full solution for acoustic radiation force on a sphere provided by Ilinskii et al.[2] based on spherical wave expansions of the incident and scattered acoustic fields:

$$F_z = \frac{i\pi}{\rho_0 c_0^2 k_0^2} \sum_{n=0}^{\infty} \sum_{m=-n}^{n} \frac{(n+m+1)(n+m)!}{(2n+1)(2n+3)(n-m)!} (A_n^* + A_{n+1} + 2A_n^* A_{n+1}) a_n^{m*} a_{n+1}^m + \text{c.c.} \tag{10}$$

The coefficients a_n^m and A_n are the spherical wave expansion coefficients of the incident and scattered fields:

$$p_{\text{in}} = \sum_{n=0}^{\infty} \sum_{m=-n}^{n} a_n^m j_n(k_0 r) P_n^m(\cos\theta) e^{im\phi}, \tag{11}$$

$$p_{\text{sc}} = \sum_{n=0}^{\infty} \sum_{m=-n}^{n} a_n^m A_n h_n^{(1)}(k_0 r) P_n^m(\cos\theta) e^{im\phi}, \tag{12}$$

where j_n and $h_n^{(1)}$ are the spherical Bessel and Hankel functions, and P_n^m are the associated Legendre polynomials. Equation (10), in combination with the expansion coefficients a_n^m and A_n for the incident and scattered waves, provides the z component of the radiation force on a spherically symmetric object of arbitrary size and composition. The coefficients A_n are obtained via solution of the full scattering problem for a sphere, and are provided by Wang et al.[5] for the case of a fluid sphere surrounded by the two concentric spherical fluid layers illustrated in Fig. 2. The coefficients a_n^m are calculated for the superposition of two plane waves.

To calculate the horizontal component of the radiation force, the z axis is taken to be parallel to the surface of the substrate, with the x axis normal to the substrate as shown in Fig. 1. The corresponding coefficients a_{nz}^m are given by the summation of coefficients for the two progressive plane wave components p_+ and p_-:

$$a_{nz}^m = a_{n+}^m + a_{n-}^m = \tfrac{1}{2} p_0 \left[1 + (-1)^{n+m}\right] (2n+1) i^n \frac{(n-m)!}{(n+m)!} P_n^m(\sin\theta_R). \tag{13}$$

The coefficients $a_{n\pm}^m$ are provided in Ref. 7. Because the sphere is centered at the origin, the substitution $z \to (z+d)$ is made in Eq. (2) to calculate the force on a sphere located at horizontal position d relative to the pressure antinode at $z = 0$. The translated coefficients then become

$$a_{nz}^m = \begin{cases} p_0 (2n+1) i^n \frac{(n-m)!}{(n+m)!} P_n^m(\sin\theta_R) \cos(k_0 d \sin\theta_R) & (n+m) \text{ even}, \\ p_0 (2n+1) i^{n+1} \frac{(n-m)!}{(n+m)!} P_n^m(\sin\theta_R) \sin(k_0 d \sin\theta_R) & (n+m) \text{ odd}. \end{cases} \tag{14}$$

Substitution of Eq. (14) into Eq. (10) along with the coefficients A_n provided by Wang et al.[5] yields the horizontal component of the radiation force, which may be compared directly with results obtained using Eq. (9). The component of the radiation force that acts in the vertical direction perpendicular to the substrate is calculated using the same procedure, but with the z axis normal to the substrate and with the surface waves propagating along the x axis. In this configuration the coefficients a_{nx}^m become

$$a_{nx}^m = \begin{cases} p_0 (2n+1) i^n \frac{(n-m)!}{(n+m)!} P_n^m(\cos\theta_R) \cos(k_0 d \sin\theta_R) & m \text{ even}, \\ p_0 (2n+1) i^{n+1} \frac{(n-m)!}{(n+m)!} P_n^m(\cos\theta_R) \sin(k_0 d \sin\theta_R) & m \text{ odd}, \end{cases} \tag{15}$$

where subscript x denotes that evaluation of Eq. (10) using Eq. (15) yields the x component of the radiation force in the direction normal to the substrate as illustrated in Fig. 1.

Material	n	ρ_n [kg/m^3]	K_n [GPa]	c_n [m/s]	R_n [μm]
Water	0	1000	2.25	1500	-
Nucleus	1	1430	3.25	1508.5	6
Cytoplasm	2	1139	2.59	1508	14
Cortical layer	3	970	2.04	1450	15

Table 1: Material properties and geometrical parameters used to model the nucleated cell considered in the present work and illustrated in Fig. 2. Values were obtained from Ref. 6.

3. RESULTS AND COMPARISONS

Results from the Born approximation are compared with the full solution for the horizontal radiation force for the cases considered by Peng et al.[6] The Born approximation is given by Eq. (9) applied to the nucleated cell modeled as a sphere surrounded by $N = 2$ concentric spherical layers as illustrated in Fig. 2. The full solution is given by Eq. (10) evaluated using the incident coefficients a_{nz}^m given in Eq. (14) and the scattering coefficients A_n provided by Wang et al.[5] The radii R_n and material properties are listed in Table 1. Unless otherwise stated, calculations employ the values given in Table 1, and the position of the cell is taken to be $\tilde{k}_0 d = \pi/4$. The radiation force is normalized by $F_0 = \pi R_3^2 p_0^2/8\rho_0 c_0^2$ in order for the quantities F_z/F_0 and F_x/F_0 presented in Figs. 3–5 to be equivalent to the dimensionless radiation forces Y_{px} and Y_{py}, respectively, appearing in Ref. 6.

Figure 3 compares results obtained from the Born approximation (solid curves) and the full solution (dashed curves) for several different configurations of cell geometry and incident field structure. Figure 3(a) corresponds to the cases considered in Fig. 10(a) of Ref. 6, with the radiation force calculated as a function of frequency for several different radii $R_3 = 30$, 25, 20, 15, and 10 μm with the inner radii determined by $R_1/R_3 = 6/15$ and $R_2/R_3 = 14/15$ and for Rayleigh angle $\theta_R = 80°$. The Born approximation and the full solution are in close agreement for all configurations of the cell geometry and for the full range of

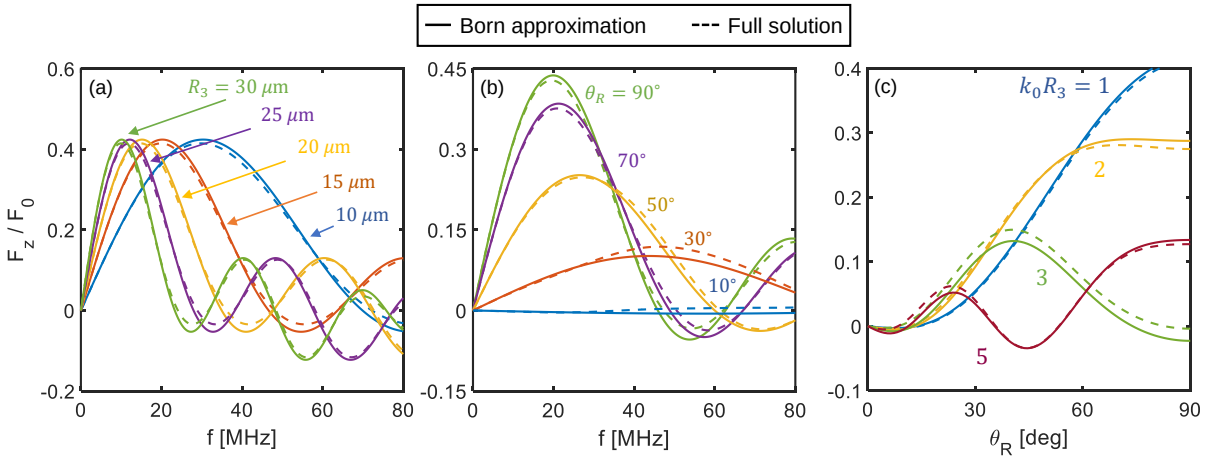

Figure 3: Comparison of the radiation force on a nucleated cell calculated using Eq. (9) (solid curves) and Eq. (10) (dashed curves) for a cell centered at $\tilde{k}_0 d = \pi/4$. In (a) the force is calculated for cells with outer radii $R_3 = 30$, 25, 20, 15, and 10 μm with fixed ratios $R_1/R_3 = 6/15$, $R_2/R_3 = 14/15$, and Rayleigh angle $\theta_R = 80°$, corresponding to Fig. 10(a) in Ref. 6. In (b) the force is calculated for Rayleigh angles $\theta_R = 90°$, 70°, 50°, 30°, and 10°, corresponding to Fig. 7(b) in Ref. 6. In (c) the force is calculated as a function of the Rayleigh angle θ_R for dimensionless frequencies $k_0 R_3 = 1$, 2, 3, and 5.

frequencies considered. For the case $R_3 = 30\ \mu\mathrm{m}$ represented by the green curves, the Born approximation remains accurate for cell diameters up to three wavelengths in the fluid at a frequency of 80 MHz. A Rayleigh angle of $\theta_R = 80°$ corresponds to an incident field that closely resembles a 1D standing wave, with strong gradients of the energy densities, resulting in the excellent performance of the Born approximation observed in Fig. 3(a).

Figure 3(b) corresponds to Fig. 7(b) in Ref. 6, with the force on the cell calculated as a function of frequency for Rayleigh angles $\theta_R = 90°$, $70°$, $50°$, $30°$, and $10°$. Here the solid curves for the Born approximation show excellent agreement for Rayleigh angles θ_R larger than about $30°$. As the Rayleigh angle becomes small, and the horizontal force due to gradients of the energy densities approaches zero, the accuracy of the Born approximation decreases. This is particularly true for $\theta_R = 10°$ (blue curves), where the Born approximation shows significant error relative to the full solution that is indiscernible at this scale due to the weak force. For this case, the incident field closely resembles a progressive plane wave traveling in the direction normal to the substrate, with weak gradients of the energy densities and associated forces in the z direction. Because cell sorting relies on the displacement of cells perpendicular to the flow direction by the horizontal radiation force, separation devices should be designed to achieve large Rayleigh angles in order to maximize the horizontal force.

In Fig. 3(c) the force is calculated as a function of the Rayleigh angle θ_R for several different frequencies described by $k_0 R_3 = 1$, 2, 3, and 5. The solid curves for the Born approximation are once again in good agreement with the dashed curves for the full solution for a wide range of angles θ_R, and for all dimensionless frequencies $k_0 R_3$. Here it is shown that although the accuracy of the Born approximation diminishes for small Rayleigh angles, both the full solution and the Born approximation approach zero at approximately the same rate. As a result, the Born approximation may remain useful for assessing the design of separation devices even when the approximation and full solution exhibit high relative error for small Rayleigh angles.

The results in Fig. 3 demonstrate that the Born approximation predicts the horizontal component of the radiation force with a high degree of accuracy for sufficiently large Rayleigh angles. However, the Born approximation does not predict the vertical component of the force exerted on the cell. While the vertical component of the force is of minor significance compared to the horizontal force in the acoustofluidic separation process, depending on the configuration of the incident field, the vertical component of the force

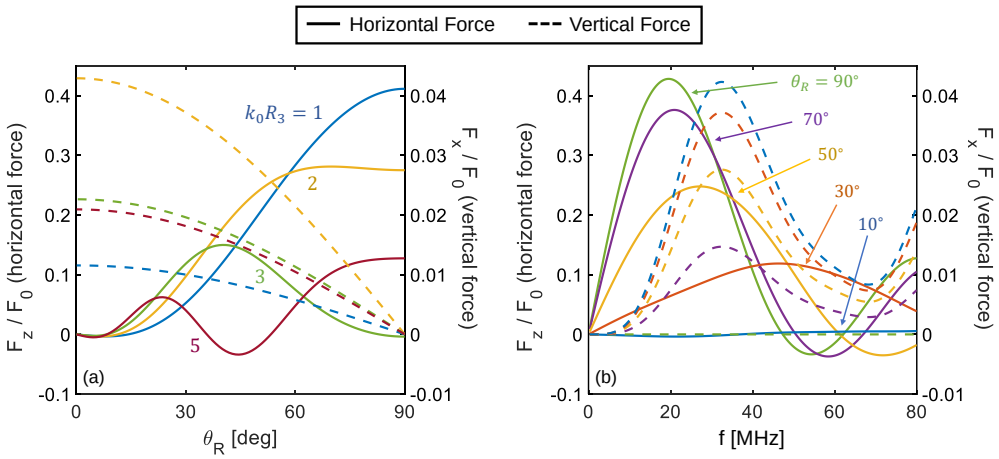

Figure 4: Comparison of the horizontal force F_z (solid curves, left vertical scale) and vertical force F_x (dashed curves, right vertical scale) calculated using Eq. (10) and the coefficients given in Eqs. (14) and (15) for $\tilde{k}_0 d = \pi/4$. The incident field configuration in Fig. 4(a) corresponds to that of Fig. 3(c), and the configuration in Fig. 4(b) corresponds to that of Fig. 3(b).

may be the dominant contribution and thus require consideration. To assess the relative significance of the two components, Fig. 4 shows the full solution for both the horizontal and vertical components of the force F_z and F_x given by Eq. (10) evaluated using the incident field coefficients given in Eqs. (14) and (15), respectively. In both figures, the horizontal force F_z is represented by the solid curves plotted relative to the left vertical axis, and the vertical force F_x is represented by the dashed curves plotted relative to the right vertical axis. The incident field configuration in Fig 4(a) corresponds to that considered in Fig. 3(c), and Fig. 4(b) corresponds to Fig. 3(b).

The comparison of the two components of the force reveals that F_z is approximately an order of magnitude larger than F_x for angles $\theta_R \gtrsim 50°$, and it is the dominant component of the force for $\theta_R \gtrsim 30°$. In the low-frequency limit ($f \lesssim 15$ MHz) in Fig. 4(b), the horizontal force remains dominant for all cases considered except $\theta_R = 10°$, represented by the blue curves. It may thus be inferred that for field configurations where the Born approximation may be expected to be accurate, the vertical component of the force may generally be considered to be negligible compared to the horizontal force.

An alternative approach to modeling the force exerted on the nucleated cell shown in Fig. 2 is to approximate the force on the inhomogeneous, multilayered sphere as the force on a sphere with homogeneous material properties averaged over the volume of the cell. For the layered sphere illustrated in Fig. 2, the homogenized density ρ_{avg} and compliance K^{-1}_{avg} are given by

$$\xi_{\text{avg}} = \frac{1}{R^3_{N+1}} \left[R^3_1 \xi_1 + \sum_{n=1}^{N} (R^3_{n+1} - R^3_n) \xi_{n+1} \right], \tag{16}$$

where ξ stands for either the density ρ or compliance K^{-1}. While there exist other homogenization methods for establishing effective material properties, any such approach that approximates the multilayered sphere as a homogeneous sphere will produce qualitatively similar results insofar as the comparison in the present work is concerned.

To illustrate the importance of accounting for inhomogeneity in the cell considered in the present work, Fig. 5 compares results obtained from the full solution given by Eq. (10) for a nucleated cell modeled as a layered sphere (solid curves), and a homogenized sphere using material properties obtained from Eq. (16) (dashed curves). The cases considered in Fig. 5 correspond to those in Fig. 3. It is observed that the

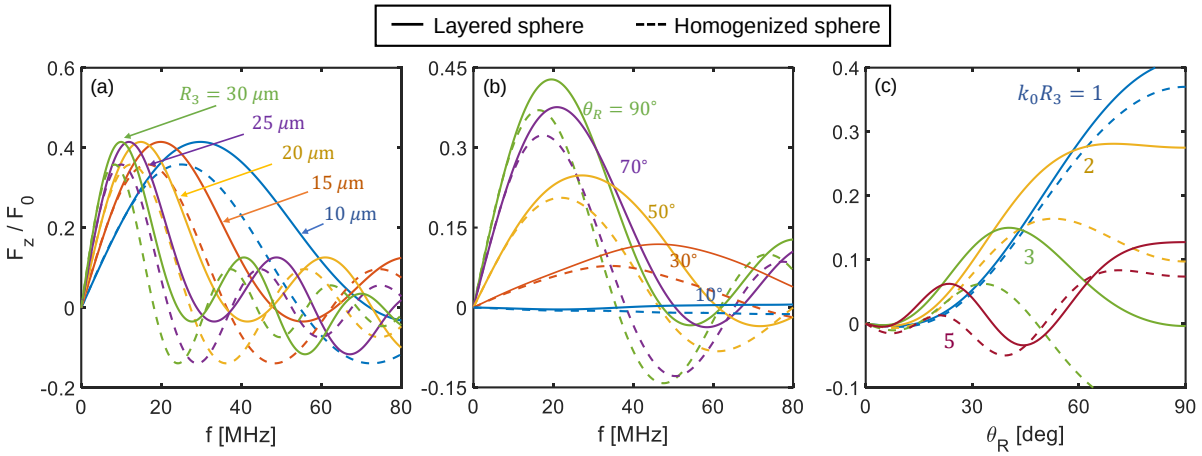

Figure 5: Comparison of results obtained using Eq. (10) for the force on a nucleated cell modeled as a layered sphere (solid curves) and a homogenized sphere with density ρ_{avg} and compliance K^{-1}_{avg} obtained from Eq. (16) (dashed curves). Figures (a), (b), and (c) correspond to the cases of cell and incident field configurations considered in Fig. 3(a), (b), and (c).

agreement between the solid and dashed curves for the inhomogeneous and homogenized cell is rather poor overall. The only exceptions are results at low frequencies, for which the length scales associated with the layered structure of the cell are much smaller than the acoustic wavelength, which represents the quasistatic limit. The approximation based on the homogenized sphere is found to agree with the complete solution for the layered sphere in Fig. 5(a) only for $k_0 R_3 \lesssim 0.7$, which for the radius $R_3 = 15\ \mu\mathrm{m}$ in Table 1 corresponds to frequencies $f \lesssim 11$ MHz.

4. CONCLUSION

Results presented here demonstrate the utility of the Born approximation of acoustic radiation force for practical problems of interest in the context of acoustofluidics. The Born approximation is applied to the case of a nucleated cell in an acoustofluidic separation device, and comparison of the analytical result with the full solution for the horizontal component of the radiation force demonstrates a high degree of accuracy over a wide range of configurations of both the cell geometry and the incident field. It is shown that the parameter space in which the Born approximation remains accurate coincides with device configurations that maximize the horizontal force that drives the sorting process in acoustofluidic separation devices, making the Born approximation a potentially useful tool for the design of separation devices. Comparison of results for a multilayered cell and a homogeneous sphere with averaged material properties underscores the importance of accounting for inhomogeneity within the object, something that is accomplished very simply in the Born approximation. Although not considered in the present work, the Born approximation can be used to model both acoustic radiation force and torque acting on objects of arbitrary shape, which may be relevant when considering irregularly shaped and inhomogeneous biological targets beyond the long-wavelength limit.

ACKNOWLEDGMENTS

Chirag A. Gokani and Thomas S. Jerome were supported by the Applied Research Laboratories Chester M. McKinney Graduate Fellowship in Acoustics.

REFERENCES

[1] M. Wu, A. Ozcelik, J. Rufo, Z. Wang, R. Fang, and T. J. Huang, "Acoustofluidic separation of cells and particles," *Microsyst. Nanoeng.* **5**, 1–18 (2019).

[2] T. S. Jerome, Yu. A. Ilinskii, E. A. Zabolotskaya, and M. F. Hamilton, "Born approximation of acoustic radiation force and torque on soft objects of arbitrary shape," *J. Acoust. Soc. Am.* **145**, 36–44 (2019).

[3] T. S. Jerome and M. F. Hamilton, "Born approximation of acoustic radiation force and torque on inhomogeneous objects," *J. Acoust. Soc. Am.* **150**, 3417–3427 (2021).

[4] T. S. Jerome, "Acoustic radiation force and torque on nonspherical objects," Ph.D. dissertation, The University of Texas at Austin, Austin, Texas (May 2022), Chaps. 3 and 4.

[5] Y.-Y. Wang, J. Yao, X.-W. Wu, D.-J. Wu, and W.-J. Liu, "Influences of the geometry and acoustic parameter on acoustic radiation forces on three-layered nucleate cells," *J. Appl. Phys.* **122**, 094902 (2017).

[6] X. Peng, W. He, F. Xin, G. M. Genin, and T. J. Lu, "Standing surface acoustic waves, and the mechanics of acoustic tweezer manipulation of eukaryotic cells," *J. Mech. Phys. Solids* **145**, 104134 (2020).

[7] P. M. Morse and H. Feshbach, *Methods of Theoretical Physics* (McGraw-Hill, New York, 1953), p. 1466.